Surface plasmon resonances in periodic and random patterns of gold nano-disks for broadband light harvesting

Yoshiaki Nishijima,[1,*] **Lorenzo Rosa,**[2] **and Saulius Juodkazis**[2,3]

[1]*Department of Electrical and Computer Engineering, Graduate School of Engineering, Yokohama National University, 79-5 Tokiwadai, Hodogaya-ku, Yokohama 240-8501, Japan*
[2]*Centre for Micro-Photonics, Faculty of Engineering and Industrial Sciences, Swinburne University of Technology, Hawthorn, VIC 3122, Australia*
[3]*Melbourne Centre for Nanofabrication, 151 Wellington Road, Clayton, VIC 3168, Australia*
[*]*nishijima@ynu.ac.jp*

Abstract: We analyze the localized surface plasmon resonance spectra of periodic square lattice arrays of gold nano-disks, and we describe numerically and experimentally the effect of disorder on resonance width, spectrum, and EM field enhancement in increasingly randomized patterns. The periodic structure shows a narrower and stronger extinction peak, conversely we observe an increase of up to $(1-2)\times 10^2$ times enhancement as the disorder is gradually introduced. This allows for simpler, lower resolution fabrication, cost-effective in light harvesting for solar cell and sensing applications. We show that dipole-dipole interactions contribute to diffract light parallel to the surface as a mean of long-range coupling between the nano-disks.

OCIS codes: (160.4236) Nanomaterials; (240.6680) Surface plasmons; (250.5403) Plasmonics; (290.4210) Multiple scattering; (220.4241) Nanostructure fabrication; (310.6628) Subwavelength structures, nanostructures.

References and links

1. S. Link and M. A. El-Sayed, "Size and temperature dependence of the plasmon absorption of colloidal gold nanoparticles," J. Phys. Chem. B **103**, 4212–4217 (1999).
2. O. Shekhah, J. Liu, R. A. Fischer, and Ch. Woll, "MOF thin films: existing and future application," Chem. Soc. Rev. **40**, 1081–1106 (2011).
3. D. M. Koller, A. Hohenau, H. Ditlbacher, N. Galler, F. Reil, F. R. Aussenegg, A. Leitner, E. J. W. List, and J. R. Krenn, "Organic plasmon-emitting diode," Nat. Photonics **2**, 684–687 (2008).
4. W. Cai, A. P. Vasudev, and M. L. Brongersma, "Electrically controlled nonlinear generation of light with plasmonics," Science, **333**, 1720–1723 (2011).
5. A. E. Miroshnichenko, S. Flach, and Y. S. Kivshar, "Fano resonances in nanoscale structures," Rev. Mod. Phys. **82**, 2257–2298 (2010).
6. D. K. Gramotnev, A. Pors, M. Willatzen, and S. I. Bozhevolnyi, "Gap-plasmon nanoantennas and bowtie resonators," Phys. Rev. B **85**, 045434 (2012).
7. V. K. Valev, N. Smisdom, A. V. Silhanek, B. De Clercq, W. Gillijns, M. Ameloot, V. V. Moshchalkov, and T. Verbiest, "Plasmonic ratchet wheels: switching circular dichroism by arranging chiral nanostructures," Nano Lett. **9**, 3945–3948 (2009).
8. M. Michaels, M. Nirmal, and L. E. Brus, "Surface enhanced raman spectroscopy of individual rhodamine 6G molecules on large Ag nanocrystals," J. Am. Chem. Soc. **121**, 9932–9939 (1999).
9. F. Lordan, J. H. Rice, B. Jose , R. J. Forster, and T. E. Keyes, "Site selective surface enhanced Raman on nanostructured cavities," Appl. Phys. Lett. **99**, 033104 (2011).

#164456 - $15.00 USD Received 9 Mar 2012; revised 26 Apr 2012; accepted 27 Apr 2012; published 4 May 2012

10. K. Ueno, S. Juodkazis, M. Mino, V. Mizeikis, and H. Misawa, "Spectral sensitivity of uniform arrays of gold nanorods to dielectric environment," J. Phys. Chem. C **111**, 4180–4184 (2007).
11. Y. Sawai, B. Takimoto, H. Nabika, K. Ajito, and K. Murakoshi "Observation of a small number of molecules at a metal nanogap arrayed on a solid surface using surface-enhanced Raman scattering," J. Am. Chem. Soc. **129**, 1658–1662 (2007).
12. Y. Nishijima, K. Ueno, Y. Yokota, K. Murakoshi, and H. Misawa, "Plasmon-assisted photocurrent generation from visible to near-infrared wavelength using a Au-nanorods/TiO_2 electrode," J. Phys. Chem. Lett. **1**, 2031–2036 (2010).
13. Y. Tsuboi, T. Shoji, N. Kitamura, M. Takase, K. Murakoshi, Y. Mizumoto, and H. Ishihara, "Optical trapping of quantum dots based on gap-mode-extinction of localized surface plasmon," Chem. Lett. **1**, 2327–2333 (2010).
14. I. M. Monirul, K. Ueno, S. Juodkazis, Y. Yokota, and H. Misawa, "Development of interdigitated array electrodes with surface-enhanced raman scattering Functionality," Anal. Sci. **26**, 13–18 (2010).
15. K. Ueno, S. Takabatake, K. Onishi, H. Itoh, Y. Nishijima, and H. Misawa, "Homogeneous nano-patterning using plasmon-assisted photolithography," Appl. Phys. Lett. **99**, 011107 (2011).
16. J. Merlein, M. Kahl, A. Zuschlag, A. Sell, A. Halm, J. Boneberg, P. Leiderer, A. Leitenstorfer, and R. Bratschitsch, "Nanomechanical control of an optical antenna," Nat. Photonics **2**, 230–233 (2008).
17. S. J. Barrow, A. M. Funston, D. E. Gomez, T. J. Davis, and P. Mulvaney, "Surface plasmon resonances in strongly coupled gold nanosphere chains from monomer to hexamer," Nano Lett. **11**, 4180–4187 (2011).
18. A. Roberts, and L. Lin, "Substrate and aspect-ratio effects in resonant nanoaperture arrays," Opt. Mater. Express **1**, 480–488 (2011).
19. K. Ueno, S. Juodkazis, V. Mizeikis, K. Sasaki, and H. Misawa, "Clusters of closely-spaced gold nanoparticles as a source of two-photon photoluminescence at visible wavelengths," Adv. Mater. **20**, 26–30 (2008).
20. T. Teranishi, M. Eguchi, M. Kanehara, and S. Gwo, "Controlled localized surface plasmon resonance wavelength for conductive nanoparticles over the ultraviolet to near-infrared region," J. Mater. Chem. **21**, 10238–10242 (2011).
21. K. Ueno, S. Juodkazis, V. Mizeikis, K. Sasaki, and H. Misawa, "Spectrally-resolved atomic-scale length variations of gold nanorods," J. Am. Chem. Soc. **128**, 14226–14227 (2006).
22. Y. K. Kim, A. J. Danner, J. J. Raftery, and K. D. Choquette, "Focused ion beam nanopatterning for optoelectronic device fabrication," IEEE J. Sel. Top. Quantum. Electron. **11**, 1292–1298 (2005).
23. M. Hu, C. Novo, A. Funston, H. Wang, H. Staleva, S. Zou, P. Mulvaney, Y. Xia, and G. V. Hartland, "Dark-field microscopy studies of single metal nanoparticles: understanding the factors that influence the linewidth of the localized surface plasmon resonance," J. Mater. Chem. **18**, 1949–1960 (2008).
24. S. Juodkazis, and L. Rosa, "Surface defect mediated electron hopping between nanoparticles separated by a nano-gap," Phys. Status Solidi - Rapid Res. Lett. **10**, 244-246 (2010).
25. W. Khunsin, B. Brian, J. Dorfmuller, M. Esslinger, R. Vogelgesang, C. Etrich, C. Rockstuhl, A. Dmitriev, and K. Kern, "Long-distance indirect excitation of nanoplasmonic resonances," Nano Lett. **11**, 2765–2769 (2011).
26. M. I. Stockman, S. V. Faleev, and D. J. Bergman, "Localization versus delocalization of surface plasmons in nanosystems: Can one state have both characteristics?" Phys. Rev. Lett. **87**, 167401 (2001).
27. T. Takasone, S. Juodkazis, Y. Kawagishi, A. Yamaguchi, S. Matsuo, H. Sakakibara, H. Nakayama, and H. Misawa, "Flexural rigidity of a single microtubule," Jpn. J. Appl. Phys. **41**, 3015–3019 (2002).
28. T. Klar, M. Perner, S. Grosse, G. von Plessen, W. Spirkl, and J. Feldmann, "Surface-plasmon resonances in single metallic nanoparticles," Phys. Rev. Lett. **80**, 4249–4252 (1998).
29. C. Sonnichsen, S. Geier, N. E. Hecker, G. von Plessen, J. Feldmann H. Ditlbacher, B. Lamprecht, J. R. Krenn, F. R. Ausseneg, V. Z-H. Chan, J. P. Spatz, and M. Moller, "Spectroscopy of single metallic nanoparticles using total internal reflection microscopy," Appl. Phys. Lett. **77**, 132355, (2000).
30. M. L. Brongersma, J. W. Hartman, and H. A. Atwater, "Electromagnetic energy transfer and switching in nanoparticle chain arrays below the diffraction limit," Phys. Rev. B **62**, R16356–R16359 (2000).
31. B. Lamprecht, G. Schider, R. T. Lechner, H. Ditlbacher, J. R. Krenn, A. Leitner, and F. R. Aussenegg, "Metal nanoparticle gratings: Influence of dipolar particle interaction on the plasmon resonance," Phys. Rev. Lett. **84**, 4721–4724 (2000).
32. W. Gotschy, K. Vonmetz, A. Leitner, and F. R. Aussenegg, "Optical dichroism of lithographically designed silver nanoparticle films," Opt. Lett. **21**, 1099–1101, (1996).
33. C. Sonnichsen, T. Franzl, T. Wilk, G. von Plessen, J. Feldmann, O. Wilson, and P. Mulvaney, "Drastic reduction of plasmon damping in gold nanorods," Phys. Rev. Lett. **88**, 077402 (2002).
34. G. V. Hartland, "Coherent vibrational motion in metal particles: Determination of the vibrational amplitude and excitation mechanism," J. Chem. Phys. **116**, 8048–8056 (2002).
35. L. Rosa, K. Sun and S. Juodkazis, "Sierpinski fractal plasmonic nanoantennas," Phys. Status Solidi - Rapid Res. Lett. **5**, 175–177 (2011).
36. X. Chen, B. Jia, J. K. Saha, B. Cai, N. Stokes, Q. Qiao, Y. Wang, Z. Shi and M. Gu, "Broadband enhancement in thin-film amorphous silicon solar cells enabled by nucleated silver nanoparticles," Nano Lett. 2012 doi: 10.1021/nl203463z (in press)
37. K. Aydin, V. E. Ferry, R. M. Briggs, and H. A. Atwater,"Broadband polarization-independent resonant light

#164456 - $15.00 USD Received 9 Mar 2012; revised 26 Apr 2012; accepted 27 Apr 2012; published 4 May 2012

absorption using ultrathin plasmonic super absorbers," Nat. Commun. **2**, 517 (2011).
38. A. K. Sarychev, V. A. Shubin, and V. M. Shalaev, "Anderson localization of surface plasmons and nonlinear optics of metal-dielectric composites," Phys. Rev. B **60** 16389–16408 (1999).
39. S. Takeda, S. Hamada, R. Peretti, P. Viktorovitch, and M. Obara, " Order to disorder optical phase transition in random photonic crystals," Appl. Phys. B **106** 95–100 (2012).
40. Z. -L. Deng, Z. -H. Li and J. -W. Dong, and H. -Z. Wang, "In-plane plasmonic modes in a quasicrystalline array of metal nanoparticles," Plasmonics **6**, 507-514 (2011).
41. K. Juodkazis, J. Juodkazytė, P. Kalinauskas, E. Jelmakas, and S. Juodkazis, "Photoelectrolysis of Water: Solar Hydrogen - Achievements and Perspectives," Opt. Express **18**, A147–A160 (2010).

1. Introduction

Localized surface plasmons are generated in nanostructures of noble metals such as gold, silver and copper, which are promising materials in the fields of optoelectronics and plasmonics [1–6]. Recently, their applications have been widely examined and reported. For instance, detection of small amounts of molecules by surface enhanced Raman scattering (SERS) spectroscopy [7–10], refractive index sensing [10], nanolithography [11], solar energy harvesting at wavelength of choice [12], optical trapping [13] and electrochemistry [14] are several active directions of research. In particular, short-range plasmon resonances in so-called "nano-gaps" [6] have been discussed because of their strong electric field enhancement ($|E|^2 \sim 10^4$) [15, 16]. Fabrication of gold nano-structures is mainly accomplished either by chemical synthesis or by semiconductor nano-fabrication methods [16–23]. Because of the difficulty to control the particle size distribution, and immobilizing them on a substrate, most of colloidal particle work has been done with random configurations.

On the other hand, nano-fabrication often involves fabricating periodic structures, because of their convenience for CAD design and numerical benchmarking with simulations using the finite-difference time-domain (FDTD) method. With nano-fabrication it is easy to control the particle size and their periodicity, hence, spectral patterns of light absorption and scattering, enhancement at nano-gaps, peculiarities of dipole-dipole interaction, and optical nonlinearities of localized surface plasmons (LSPRs) have been demonstrated and explored [6, 19]. However, the facility costs are increasing when fabrication resolution of nano-gaps down to few nanometers is required. Moreover, the required high-voltage ($\geq$ 100 keV) electron beam lithography is known to create subsurface defects [24] and, e.g., can compromise performance and long time stability of solar cells. One strongly desired feature is a large enhancement factor with low fabrication resolution (leading to low-cost device fabrication as a result).

In this study, we show long-range interactions during the transition between order and disorder in low-resolution fabricated gold nano-particles, and the transition effect on the optical properties of such patterns. Dipole-dipole long-range interactions between perfectly ordered nano-particle arrays [31] and fully disordered [25, 26] patterns of plasmonic nano-particles have been examined. The ordered patterns show distinct extinction resonances scalable with the period and spectrally red-shifted, because of the phase alignment of scattered fields between neighboring particles [31]. In disordered patterns it is shown that the dipole-dipole interaction virtually disappears when $Period/Diameter > 2.5$ [25]. Here, we show how by tuning the degree of randomness it is possible to control the extinction properties of the patterns, through the strong dipolar interactions arising from the shift between evanescence and radiation of different light diffraction orders. The long-range interaction of nano-particles observed in the extinction spectrum is maximum at the critical period, when diffraction orders radiates and higher orders are traveling along the surface in a grazing angle mode. The optical properties (extinction spectra and field enhancement) of gold nano-disk arrays are systematically studied experimentally and numerically for the first time during the order-to-disorder evolution, which is introduced in a controlled way through a random walk algorithm.

#164456 - $15.00 USD Received 9 Mar 2012; revised 26 Apr 2012; accepted 27 Apr 2012; published 4 May 2012

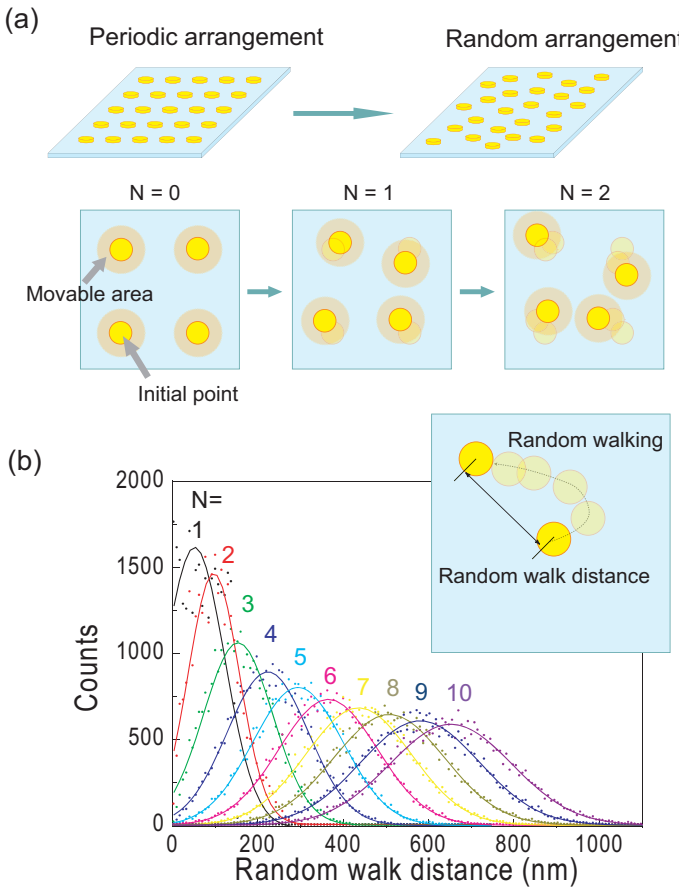

Fig. 1. (a) Method description for random configuration preparation. (b) Statistical distribution of nano-disk distance from the initial configuration, from the first to tenth random-walk step (a numerical result).

2. Samples and methods

Patterns of gold nano-disks are CAD generated by the random-walk method starting from a perfectly periodic arrangement. A schematic illustration of the random structure preparation is shown in Fig. 1(a), where the centers of the disks are allowed to move up to 150 nm beyond the disk diameter for each step, and the random walk is iterated for N = 10 steps. The statistical distribution of the step-by-step nano-disks' distances from the initial configuration is shown in Fig. 1(b), where the random-walk distances are well fit by Gaussian profiles with average distance increasing with the step number. Random walks have been generated for initial periodicities ranging from 450 nm to 800 nm, with disks diameters of $d = 150$, 200, and 250 nm. After the final random walk step, the area covered by the nano-disks is expanded by about 0.17%, and 1% of the disks overlap (which is allowed by the algorithm design); correspondingly, the gold area coverage decreases by 1.01 times.

The arrays have been fabricated by electron beam (EB) lithography lift-off techniques. EB resist (ZEP520A, Zeon) has been coated on glass substrate by spin coating (3000 rpm, 60 s). After baking at 180°C for 2 min., the surface of resist has been coated with charge dissipating agent for EB lithography (ESPACER, Showa Denko). The EB drawing has been carried out

#164456 - $15.00 USD Received 9 Mar 2012; revised 26 Apr 2012; accepted 27 Apr 2012; published 4 May 2012

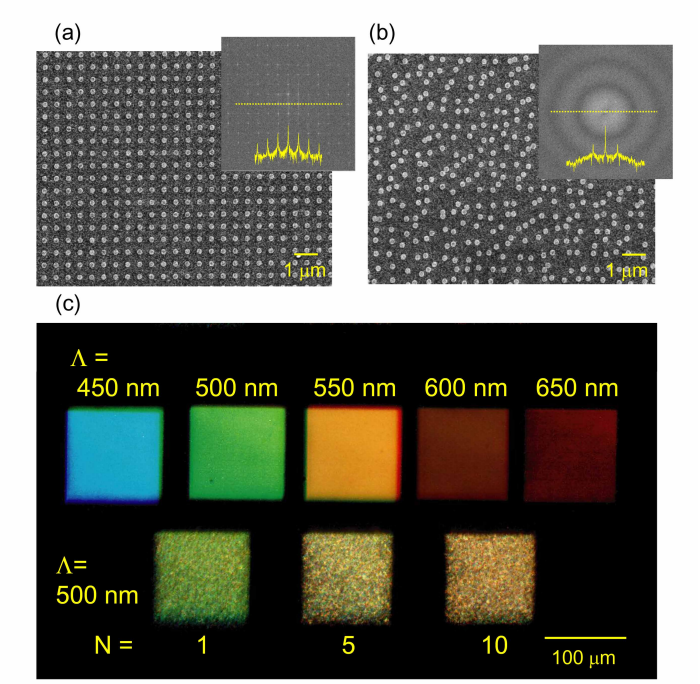

Fig. 2. SEM images of (a) periodic structure with period Λ = 500 nm and (b) random configuration with mean random-walk distance of 669 nm (N = 10). Inset figures are FFT image of SEM pictures. (c) Dark-field optical microphotograph of gold nano-structures arrays. Upper layer samples are periodic structures with $\Lambda = 450, 500, 550, 600, 650$ nm periodicity, respectively. Lower ones are random structures with 500 nm periodicity and random walk numbers N = 1, 5, and 10, respectively.

with 50 kV acceleration voltage on a EB lithography system (ELS 7500EX, Elionix). After developing (ZEP-RD, Zeon) for 1 min and rinsing by ZMD-B for 15 s twice, a 2 nm of Cr and 25 nm of Au have been deposited using a vacuum evaporation system (ULVAC). After that, a lift-off has been performed in a resist remover (ZDMAC, Zeon) with heating up to 60°C for 3 min., rinsed by acetone and methanol. The structures have been imaged with a scanning electron microscope (SEM - JSM-7500F, JEOL), and the transmission spectra have been measured with a confocal microscope system, composed of a microscope ($10^{\times}$ objective $NA = 0.5$, pinhole diameter 0.1 mm, Optiphoto, Nikon) and an optical spectrum analyzer (Q8381A, Advantest).

The 3D FDTD simulation employs a domain whose starting size is $7 \times 7 \times 0.5\ \mu\text{m}^3$, and the nano-disks are automatically placed according to the designed layouts used in fabrication. Patterns are illuminated by a plane wave source shining from the air side towards the negative z-direction. Perfectly matched layers (PMLs) are used on the z-axis boundaries, while periodic boundaries conditions (PBCs) are placed on the x- and y-axis ones. The PBC positions are first adjusted to match the periodicity of the N = 0 layout, which is enlarged to a size of 11×11 periods to make boundary effects negligible with respect to the nano-disks response. The PBCs are necessary to avoid diffraction of the plane wave source at the domain edge, however when the structure is randomized they introduce a periodicity. When the PBC positions are slightly adjusted to avoid introducing asymmetric disks and to make the average disk spacing

#164456 - $15.00 USD Received 9 Mar 2012; revised 26 Apr 2012; accepted 27 Apr 2012; published 4 May 2012

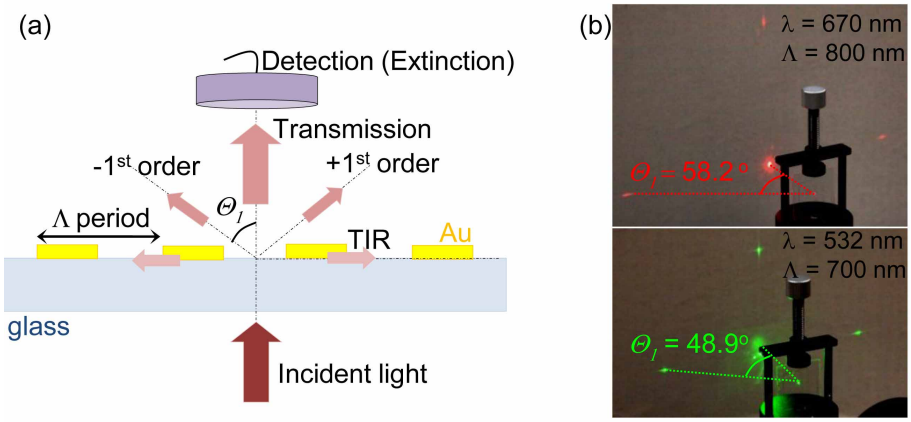

Fig. 3. (a) Schematic depiction of extinction measurements and coupling of diffracted light along surface via radiation at grazing angle. (b) Photos of the diffraction pattern in transmission, 2nd-order is in grazing mode and propagates along the surface (recognizable by coloring of the cover glass edges).

uniform, their influence has been found negligible due to the large number of disks included in the domain. The reflected and transmitted power is collected by two monitors at opposite ends of the domain; due to the periodicity, the monitors collect the total power over all the diffraction orders. The effect of staircase approximation is addressed by reducing the square mesh size around the nano-disks to about 2 nm (or about $\lambda/500$), forcing the use of a dedicated machine on a 3D mesh totaling around 1.5 million mesh points. The simulation times ranged from 1 to 3 hours and total memory occupancy ranged from 10 to 18 GB, with increasing times and memory according to greater mesh complexity for increasing random-walk step. The simulations have been performed on the Green machine, a 150-node supercomputer with 8-core calculation nodes, each carrying 16 GB memory. Workload has been subdivided by employing one 8-node cluster per simulation.

3. Results and discussion

3.1. Optical properties and grating coupling

Figures 2(a) and 2(b) show SEM images of fabricated gold nano-disks together with their 2D fast Fourier transform (FFT) spatial distributions in the insets. With respect to the periodic structures, the random structures for N = 10 have clearly lost their periodicity. The FFT retains periodicity peaks up to third order for N = 0, 1, and 2, while for greater number of steps only zero- and first-order peaks remain, indicating a randomness increase of the disk array for increasing step N, although weak periodic features persist even after many steps. After several steps, some of the nano-disks start to cluster within a few nanometers or overlap, a situation that models well the aggregates reached by self-assembling nano-particles, typically obtained in experiments of chemical gold nano-particle synthesis. These features are also revealed by dark-field optical imaging, a scattering measurements technique for single nano-particle spectroscopy [19, 23, 27–29]. Although the nano-disk extinction spectra peak in the near-infrared (see Figs. 3 and 4(a)), scattering peaks in the visible band, ranging from blue to red color. Since in the dark field imaging only the scattered light is collected (transmission is not detected) the periodic array of gold nano-disks act as a diffraction grating and only the color of the diffracted light is apparent in the image; strong scattering occurs at wavelengths close to wavelength of

#164456 - $15.00 USD Received 9 Mar 2012; revised 26 Apr 2012; accepted 27 Apr 2012; published 4 May 2012

light. On the other hand, the scattering color becomes gradually blurred with increasing step N and increase of randomness (bottom row in Fig. 2(c)). The N = 5 and N = 10 dark-field images show a slightly reddish color, with a white background. The red color corresponds to the gold plasmonic resonance, and the white color is due to multi-wavelength distributed scattering caused by the randomness.

Figure 3 shows schematically how the higher order diffraction is coupled into light directed along the surface at grazing angle in case of critical period Λ. The experimentally measured 1st-order diffraction angles, $\Theta_{\pm 1}$, are shown in Fig. 3(b). It is noteworthy that in the case of optically thick not plasmonic pattern, the diffraction orders would gradually disappear in transmission as the period becomes small and closer to the wavelength of incident light according to the grating formula $n\lambda = \Lambda \sin\Theta_n$, here n is the order of diffraction maxima, Λ is the period, and λ is the wavelength of incident light. Since gold cylinders are only 40-nm-thick and transmission is mediated by plasmons, an efficient diffraction in transmission has been observed (Fig. 3(b)). The 2nd-order diffraction is exactly at grazing angle; it directs light along the surface and contributes to surface plasmon excitation along the array of Au-cylinders [30]. This contributes to the light enhancement by individual nano-disks. In this way even far away separated nano-disks are coupled at specific wavelengths when diffraction enters grazing mode; an extinction spectrum shows the corresponding peak. The 1st-order diffraction also contributes to the extinction losses (see, Fig. 3(a)) but it does not contribute to the light enhancement since light is escaping surface and nano-particles. Light propagation from glass to air is favorable for grazing angle coupling. For the quantitative results, the electromagnetic field enhancement is estimated by FDTD analysis in Sec. 3.3.

3.2. Experimental extinction spectra

The plasmonic resonances of the periodic/random structures have been characterized by measuring their extinction spectra for periodicity intervals between 450 and 800 nm, and disk diameters from 150 to 250 nm, in 50 nm intervals. Typical extinction spectra of periodic arrays are shown in Fig. 4. With increasing periodicity, the extinction peak value decreases, as the density of gold nano-disks decreases, and the peak wavelength is red-shifted. As for the cause of this red-shift, the near-field coupling of gold nano-particles pairs is efficient at few tens nanometers distance and gradually vanishes as $\Lambda/d > 2.5$ [25]. The red shift (Fig. 4) shows that dipole-dipole interaction is stronger as the separation between the particles increases in the periodic pattern [25]. In fact, as observed in FDTD calculations, at the particular wavelength, the electromagnetic field enhancement also increases (see, Sec. on simulations). According to refs. [25, 31, 32], the red shift is related to the dipole-dipole interaction, is linked to the phase of plasmonic field, and its strength can be estimated from the bandwidth of plasmonic resonance. The results shown in Fig. 4 for the periodic patterns are in good agreement with predictions reported in ref. [31] for the longer wavelengths (emission to air [31]). At the shorter wavelengths, the feature at critical period [31] due to coherent plasmon scattering and emission into substrate was out of spectral range of our detection (Fig. 4), but can be recognized in Figs. 2(c) and 3 when propagating diffraction orders forms the image and recognizable by color of the extinction maxima (direct transmission is canceled in the dark-field microscopy mode).

The difference between periodic and random arrays is analyzed in Fig. 5(a), where the random-walk effect on the spectra causes linearly decreasing extinction peak values with increasing average random-walk distance, with a blue-shift of the peak wavelength as the in-phase matching of the scattered fields of the single nano-particles is progressively disrupted (see Fig. 5(b)). Extinction wavelengths are almost the same in all samples. This result indicates that the quality Q-factor of the random arrays is strongly linked to that of the periodic ones. It is noteworthy that what we discuss further in terms of the Q-factor and dephasing time,

#164456 - $15.00 USD Received 9 Mar 2012; revised 26 Apr 2012; accepted 27 Apr 2012; published 4 May 2012

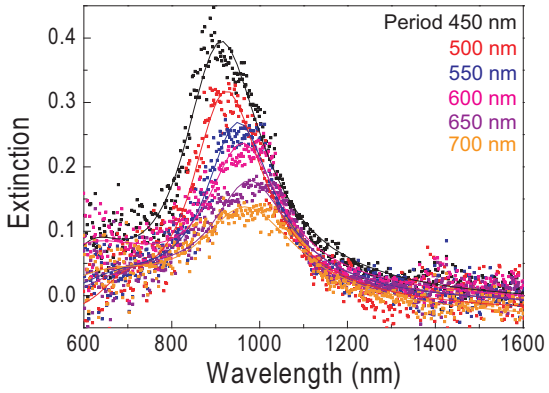

Fig. 4. Experimental extinction spectra of periodic arrays with periods between $\Lambda = 450$ nm and 700 nm. Diameter of nano-cylinders $d = 150$ nm.

T_2 (defined by the FWHM of the extinction peak) are affected by diffraction losses (Fig. 3). Hence, a strong and narrow extinction peak (consequently large T_2) does not necessary mean that nano-particles are less interacting, but rather contribute to strong diffraction (e.g., Fig. 5(b)) as discussed below.

The dephasing time of the plasmon resonance $T_2 = 2\bar{h}/\Gamma$, where Γ is the FWHM of the resonance peak [33, 34] and $\bar{h}$ is the reduced Planck constant. Results are plotted in Fig. 5(b) as a function of the average random-walk distance, that is the maximum peak of the Gaussian fit in Fig. 1(b): the dephasing time is inversely proportional to the average distance. Therefore, the FWHM of extinction resonance is linearly increasing as random walk progresses, however, the area under the extinction curve is almost constant, with a linear reduction of the observed extinction maximum. Interestingly, all the random structures converge towards the same dephasing time $T_\infty = 3.7$ fs (defined as the dephasing time at N = ∞, or the time in completely random patterns). On the other hand, the periodic dephasing time varies considerably with the period, as can be seen from appearance in Fig. 3. The dephasing is related to the LSPR losses due to interaction between nano-particles in the pattern as well as due to diffraction. By controlling the average intra-particle distance is it possible to tune the width of the extinction peak.

We also performed dephasing measurements on the samples with different nano-disk diameters. The ratio of dephasing time between periodic and random (at N = ∞) arrays has been plotted in Fig. 6: the maximum dephasing time is strongly linked to the square lattice period. There is an optimal period for each disk diameter: for 150 nm diameter it is 550 nm, for 200 nm diameter it is 650 nm, and for 250 nm diameter it is 750 nm, respectively. Note, those wavelengths corresponds to strong diffraction responsible for the scattered/diffracted light in dark-field imaging (see, Fig. 2(c)) and are explained by the discussed mechanism shown in Fig. 3(a). This value is connected to the LSPR wavelength, namely, when the LSPR wavelength has shifted to longer wavelength because of the increasing disk diameter, the diffraction losses due to effective grating also shifts to longer wavelengths (Fig. 1(b)). As a result, the extinction value, Q-factor, and dephasing time, T_2, measured spectroscopically have maxima related to the plasmonic properties as well as to the light diffraction losses due to pattern periodicity.

In the case of a random structure, each nano-disk has slightly different resonance wavelength because of different long-range interaction, thus the randomly-scattered light is spread over all wavelengths, as shown in Fig. 2(c) and LSPR spectra seem to have broader and lower extinction and shorter dephasing time. Spectrally broader plasmon resonances are favorable in practical

#164456 - $15.00 USD Received 9 Mar 2012; revised 26 Apr 2012; accepted 27 Apr 2012; published 4 May 2012

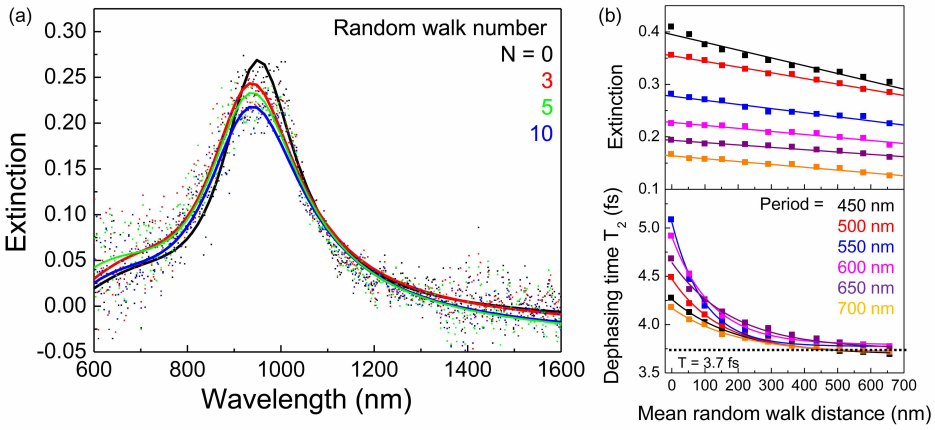

Fig. 5. Random-walk induced changes of experimentally measured extinction; diameter of nano-disk is $d = 150$ nm. (a) Extinction spectra for Λ = 550 nm with N = 0, 3, 5, and 10, respectively. (b) Dependence of the extinction maximum and of the dephasing time, T_2 (extinction at peak wavelength) on the random-walk distance.

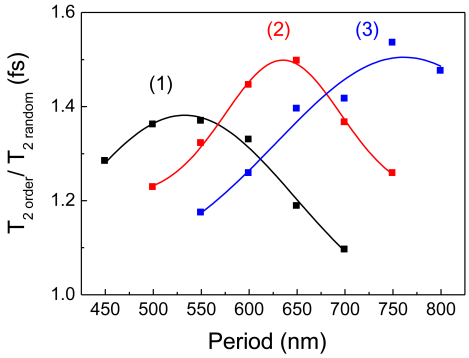

Fig. 6. Experimental dephasing time ratios of periodic structures relative to random structures for different diameters $d = 150$ (1), 200 (2), and 250 nm (3), respectively.

light harvesting applications [35–37]. In contrast, periodic nano-disk arrays show an increase of the LSPR resonance, relative to the random configuration, larger Q-factor and longer dephasing time T_2 (Fig. 6).

3.3. 3D-FDTD analysis of light field enhancement

Field enhancement calculation is then confirmed by simulation with 3D-FDTD software Lumerical, looking for extinction and E-field enhancement values around the peak wavelength. Calculation has been performed on a 6 $\times$6 μm wide domain for the periodic ordered and random structures with disks' arrangement as taken from the CAD design. The arrays are illuminated by a x-polarized plane wave source between 600 and 1000 nm wavelength. The periodic array shown in Fig. 7(b) has periodicity of 600 nm and nano-disk diameter of 160 nm (the designed diameter was $d = 150$ nm). It can be seen in Fig. 7(a) that the maximum extinction is

#164456 - $15.00 USD Received 9 Mar 2012; revised 26 Apr 2012; accepted 27 Apr 2012; published 4 May 2012

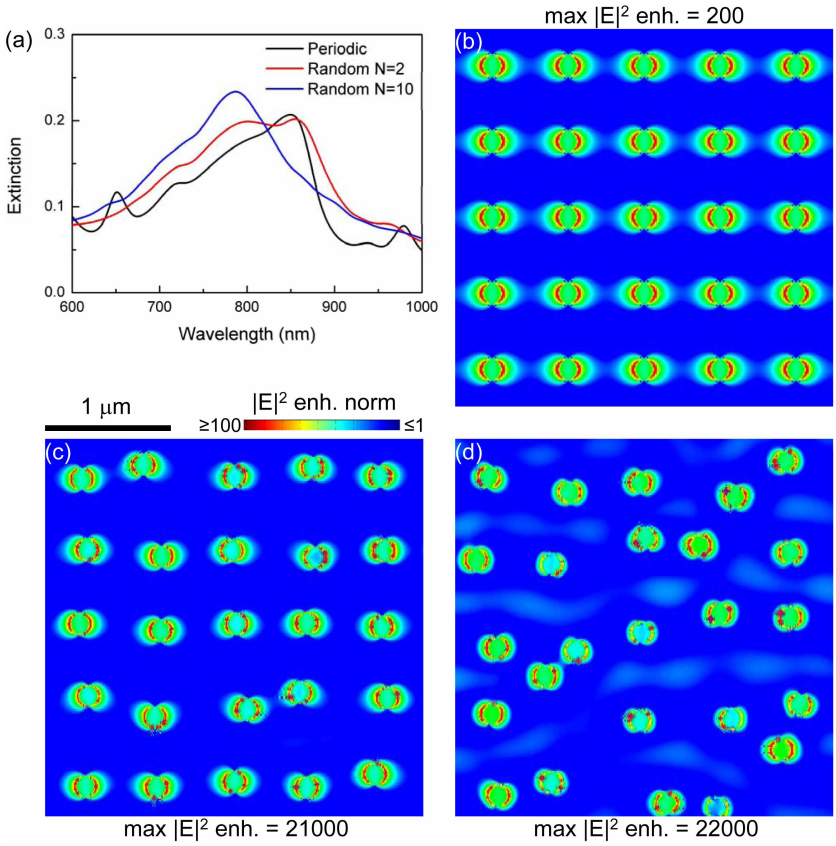

Fig. 7. 3D-FDTD calculations: (a) normalized extinction spectrum for periodic and random-walk nano-disk array (periodicity 600 nm, diameter 160 nm) and log-plots of normalized E-field enhancement on top of the nano-disks for (b) periodic array (λ = 850 nm), (c) random-walk with N = 2 (λ = 850 nm), and (d) random-walk with N = 10 (λ = 790 nm). The maximum enhancements are: 200 (b), 2.1×10^4 (c), 2.2×10^4 (d).

around 0.2, which confirms the experimental result, but the peak is moved to 850 nm because of the smaller disks. The maximum field enhancement obtained is 200 at the edges of the disks and the field distribution is highly symmetric. The figure shows the enhancement at 850 nm wavelengths in logarithmic scale ranging from 1 to 100, depicting quite broad hot-spots due to regular coupling.

Figures 7(c) and 7(d) show the random walk configuration, in the same conditions as before. For N = 2 it can be seen that the peak tends to split in two, originating a second resonance at shorter wavelength. The enhancement figure shows a more random pattern, with fewer hot-spots, but much more focused. For longer random walk with N = 10, the first peak disappears and it can be seen that the maximum extinction is still around 0.2 but above the periodic value, and the peak is narrower and is moved to slightly shorter wavelength at 790 nm. These trends are all confirmed by the experimental results. E-field enhancement is two orders of magnitude higher at 2×10^4 for both N = 2 and N = 10, whose enhancement distribution is shown in the figure, and many peaks exist, unevenly distributed because of the random configuration: due to distribution of disk distances there are many coupled resonances at different wavelengths, while the enhancement tends to increase when disks are closer together and to decrease where

#164456 - $15.00 USD Received 9 Mar 2012; revised 26 Apr 2012; accepted 27 Apr 2012; published 4 May 2012

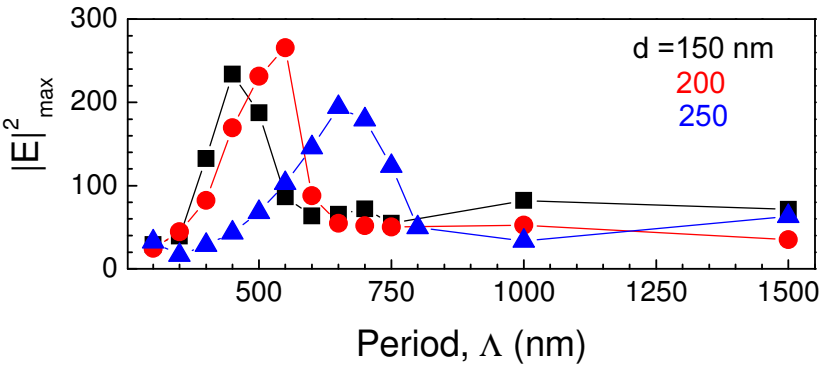

Fig. 8. Light field enhancement for the periodic nano-cylinders of diameter, *d*, calculated by 3D-FDTD method.thickness of Ag was 25 nm; the enhancement maximum is plotted at the extinction peak.

the average distance is greater. This shows that after the very first random walk steps (N = 2) towards a disordered pattern, strong enhancement hot-spots occur, while the orientation of the single dipolar resonances also consistently increases in randomness [25, 26, 31].

This confirms the correlation of lower intensity and red-shift of light emission of the samples shown in Fig. 2(c) as the periodic distance increases, and the granular nature of the coloring in the random samples, whose luminosity well correlates with the periodic samples having the same average hue. The dual-peak nature well accounts for the characteristic two-color granularity that is apparent from the sample photos. The phenomenon of hot-spot occurrence is, most likely, related to the Anderson localization which occurs in random [38, 39] and quasi-crystal arrangement of plasmonic nanoparticles [40]. Experimental investigation of light localization in 2D plasmonic patterns is challenging since the in-plane light scattering and propagation has to be measured and decoupled from diffraction (see, Fig. 3) usually by near-field optical methods and scaling properties of scattering on disorder and particle separation has to be determined. FDTD simulations of the energy dissipation occurring perpendicularly to the incident light can be modeled and is planned as a next step of our study. The critical separation of nanoparticles for localization of light at certain wavelengths and creation of hot spots will be numerically investigated and compared with theoretical predictions [38].

Figure 8 shows simulated light field enhancement dependence on the period Λ for several diameter nano-cylinders. The structure was illuminated from the air side for a gold layer of 15 nm. For memory reasons, the simulation was performed on a single nano-cylinder, whose response was extended to the full array by suitably placed periodic boundary conditions on the *x* and *y* boundaries. A strong enhancement was observed at the visible wavelength and it fades out for the large periods. This observed tendency of the strongest enhancement is consistent with reported experimental extinction dependence on the period [31].

4. Conclusion

In this study, we have demonstrated the effect of periodic and random particle patterns on the plasmonic resonance. An increase of extinction and a broader plasmon resonance occur at the increasing disorder and can be accounted by a grating-like losses due to diffraction. FDTD calculations show an augmentation of the enhancement by more than two order of magnitude for the random configuration of nano-disks, however, those hot-spots are more sparsely distributed on the surface. Previously, such strong enhancements were only been obtained with nano-gap

#164456 - $15.00 USD Received 9 Mar 2012; revised 26 Apr 2012; accepted 27 Apr 2012; published 4 May 2012

structures (via short-range dipole-dipole interaction) but could not be seen in patterns with large intra-particle distance.

Theoretical simulation and experimental results shown in this paper should be also applicable not only to top-down plasmonic technologies, but also to self-assembling patterns. The random configuration is one of the most inexpensive ways to place nano-particles on the substrate, favored for industrials application of LSPR in spectral control of light harvesting for solar cells [12, 41] and sensing [35–37].

Acknowledgments

YN gratefully thanks Prof. Toshihiko Baba of Yokohama National University for fruitful discussions and support for facilities, and Prof. Hiroaki Misawa (RIES Hokkaido Univ.) for fruitful discussions; YN has learned the fabrication methods during PhD studies at Hokkaido Univ. This work was financially supported by research grants from Yokohama Academic Foundation and the Research Foundation for Opt-Science and Technology.

#164456 - $15.00 USD Received 9 Mar 2012; revised 26 Apr 2012; accepted 27 Apr 2012; published 4 May 2012